Acta Cryst. (1981). A**37**, 105–119

The Geometry of X-ray Diffraction from Extended-Face Single Crystals

BY G. J. MCINTYRE*

School of Physics, University of Melbourne, Parkville 3052, *Australia*

(*Received* 5 *October* 1979; *accepted* 19 *August* 1980)

Abstract

An analytical method for the description and analysis in real space of X-ray Bragg reflections from extended-face crystals is presented. The method is applied to discuss the stationary-crystal diffracted-beam images in both the symmetric and asymmetric reflection positions, to analyse the ω and $\omega:2\theta$ scan modes and to derive the optimum coupling between the detector and crystal motions for an equatorial-plane diffractometer. In practice, the optimum scan mode would require the use of a receiving aperture inclined with respect to the diffraction plane, the angle of inclination being dependent on the diffractometer setting angles. It is concluded that the $\omega:2\theta$ scan mode is most suitable for routine data collection. Experimental images of the diffracted beam illustrate clearly the validity and usefulness of the mathematical description.

1. Introduction

The introduction of the 'Eulerian cradle' goniostat by Furnas & Harker (1955) began a period of considerable development in the use of counter diffractometers for the measurement of the intensities of X-ray reflections from single crystals. Since the majority of the diffractometer measurements have been carried out using small single crystals bathed entirely in the X-ray beam, the theory of the measurement of integrated intensities and the studies of the various geometrical considerations necessary in the diffraction experiment, although extensive, have been largely restricted to such crystals (see, for example, Alexander & Smith, 1962; Burbank, 1964; Arndt & Willis, 1966; Ladell & Spielberg, 1966; Kheiker, 1969; Werner, 1972; Einstein, 1974).

The early investigations of X-ray intensities were made almost exclusively with extended-face crystals. Although a solution to the absorption correction problem was suggested by Bragg (1914), the lack of a χ-circle limited further development of the extended-face technique. With the emphasis then being upon powder samples or small specimens bathed in the beam, the use of extended-face crystals was only occasionally reported, principally with regard to the measurement of refractive indices (*e.g.* Field & Lindsay, 1937) and to monochromators (*e.g.* Gay, Hirsch & Keller, 1952). Use of the χ circle on modern three- and four-circle diffractometers permits symmetric Bragg diffraction from planes inclined to the surface of the crystal and thus obviates the absorption correction problem (Mair, Prager & Barnea, 1971*a*,*b*).

The use of extended-face crystals has been advocated for accurate determination of experimental structure factors (Barnea, 1975). They have been used in cases where suitable small crystals are difficult to obtain (Harada, Pedersen & Barnea, 1970), for very accurate measurement, particularly of weak reflections (Trucano & Batterman, 1972; Hollenberg & Batterman, 1974; Mair & Barnea, 1975; Bilderback & Colella, 1976; Freeman, Mair & Barnea, 1977; Whiteley, Moss & Barnea, 1978; Merisalo & Järvinen, 1978; Merisalo, Järvinen & Kurittu, 1978; Merisalo, Peljo & Soininen, 1978) and for absolute polarity determination (Liminga, Chomnilpan & Abrahams, 1978).

The main advantages offered by the use of extended-face crystals for X-ray intensity measurements are:

(1) The absorption correction, even in the general asymmetric reflection position, is very simple; in fact, in relative intensity measurements, the value of the absorption coefficient need not be known (Mair, Prager & Barnea, 1971*a*,*b*; Mathieson, 1975).

(2) Usually only one surface of the crystal is used and the diffracting region is nearly the same for all reflections. This minimizes systematic errors due to perfectional inhomogeneities. There is, however, a limitation on the number of observable reflections imposed by the dimensions of both the crystal face and the primary beam (McIntyre, 1981).

(3) Because the crystal intercepts the entire incident beam, diffracted intensities are high, decreasing measuring time and facilitating the measurement of weak reflections. Inhomogeneity in the incident beam is only a problem with regard to orientation determination.

(4) The simple geometry makes absolute measurement with extended-face crystals far easier than with small crystals bathed in the beam.

* Present address: Institute of Chemistry, University of Uppsala, Box 531, S-751 21, Uppsala, Sweden.

0567-7394/81/010105-15$01.00

These advantages can only be confidently realized with a thorough understanding of the various geometric factors that affect the measurement.

This paper presents an analytical method for describing the geometric optics of X-ray reflections from extended-face crystals. We apply this method first to derive the diffracted-beam images for a stationary crystal and secondly to analyze the ω, $\omega:2\theta$ and the general $\omega:g\theta$ scan modes and their respective receiving-aperture widths.

Although the use of crystal-monochromatized radiation is recommended for accurate intensity measurements (Ladell & Spielberg, 1966), we restrict the present study to the case of an incident beam taken directly off the focal spot of an X-ray tube. The X-ray spectrum of the beam consists of the $K\alpha$ doublet on a continuous background of white radiation. The formulae describing the diffracted-beam images are then valid for both unfiltered and filtered (by β or balanced filters) radiation. Since the area of the crystal surface irradiated is generally so large that it is the predominant factor determining the shape and size of the diffracted image, we assume, unless otherwise stated, that: (1) the intrinsic diffraction profile is a δ function; (2) there is no mosaic spread; (3) absorption is infinite; (4) the angle subtended by the source at the crystal is zero; and (5) the characteristic X-ray lines have negligible width. Expressions for the scan angle and receiving-aperture dimensions when these assumptions are relaxed are presented in the discussion. For brevity and clarity matrix arithmetic is used as much as possible in the geometrical description.

A preliminary account of this work has been presented by McIntyre & Barnea (1978).

2. Definition of diffractometer angles

The particular four-circle diffractometer, for which we shall derive the expressions describing the optics, is illustrated schematically in Fig. 1. The diffraction plane is defined as the plane perpendicular to the instrument axis and passing through the instrument centre. Both the 2θ and ω axes are collinear with the instrument axis. The 2θ axis defines the position of the detector lying in the diffraction plane relative to the ideal incident beam direction. The χ axis lies in the diffraction plane and makes an angle ω with the ideal incident beam direction. The plane perpendicular to the χ axis and passing through the instrument centre includes the χ circle. The φ axis lies in the χ circle at an angle χ to the instrument axis. The extended-face specimen is rigidly attached to the φ shaft and is assumed to be aligned such that the face is perpendicular to the φ axis and passes through the centre of the instrument.

The conventions adopted concerning the senses of rotation and origins of θ, ω and χ and the sense of rotation of φ are indicated in Fig. 1. The origin of φ may in general be chosen arbitrarily; in this discussion we assume that, at the zero position of φ, the scattering vector **S** of the reflection being considered, the unit vector normal to the crystal face **n** and the instrument axis **z** are coplanar, and $\mathbf{z} \times \mathbf{n}$ has the same sense as $\mathbf{n} \times \mathbf{S}$.

In addition to the diffractometer angles, define α_0 to be the angle between the scattering vector and the normal to the crystal face. The direction of **n** is determined by χ and ω; the direction of **S** relative to **n** is described by α_0 and φ (Fig. 1).

The expressions derived in this paper are valid for instruments with other conventions if the appropriate transformations are made.

3. Basic beam equations

3.1. *Definition of coordinate systems*

We define several right-handed Cartesian coordinate systems $X_i Y_i Z_i$, all of which have origin at the centre of the instrument and are coincident when all the setting angles 2θ, φ, ω and χ and the crystal angle α_0 are zero. All rotations used to define the different systems are right-handed rotations about their respective axes.

Define the *laboratory system* $X_1 Y_1 Z_1$ in the following way: X_1 to be along the ideal incident beam and directed away from the source; Z_1 to be collinear with the instrument axis and directed upwards. The *2θ-axis system*, $X_2 Y_2 Z_2$, rigidly attached to the 2θ axis, is obtained from $X_1 Y_1 Z_1$ by a 2θ rotation about Z_1. The detector face lies in the plane $X_2 = t$. The *χ-axis system*, $X_5 Y_5 Z_5$, is attached to the χ axis and is related to

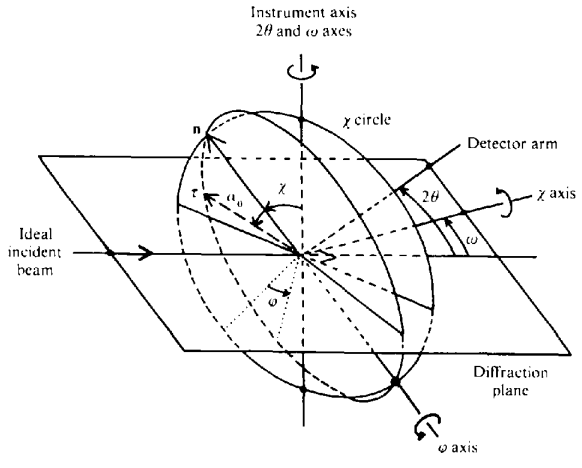

Fig. 1. Geometry of the four-circle diffractometer. All rotations indicated are positive and in the first quadrant. τ is the unit vector with the same sense and direction as **S**, and does not necessarily lie in the diffraction plane.

$X_1 Y_1 Z_1$ by a rotation about Z_1 of ω to give $X_4 Y_4 Z_4$ followed by a rotation about X_4 of $(90° - \chi)$. Thus, X_5 lies in the diffraction plane, collinear with the χ axis and Y_5 is coincident with **n**. The *diffracting-plane system*, $X_3 Y_3 Z_3$, is derived from $X_5 Y_5 Z_5$ by a rotation about Y_5 of $(-\varphi)$ to give $X_6 Y_6 Z_6$, followed by a rotation about X_6 of $(-\alpha_0)$. The axis Y_3 is then coincident with **S**.

The vector $\mathbf{X}_i$ in the system $X_i Y_i Z_i$ is transformed to $\mathbf{X}_j$ in the system $X_j Y_j Z_j$ by using the rotation matrix $\mathbf{R}_{ji}$ as follows:

$$\mathbf{X}_j = \mathbf{R}_{ji}\,\mathbf{X}_i.$$

Because of the orthonormality of the transformations, the inverse transformation is $\mathbf{R}_{ij} = \mathbf{R}_{ji}^{-1} = \mathbf{R}_{ji}^t$, where $\mathbf{R}_{ji}^t$ is the transpose matrix of $\mathbf{R}_{ji}$. Furthermore, $\mathbf{R}_{ji} = \mathbf{R}_{jk}\,\mathbf{R}_{ki}$. The matrices that we shall require are

$$\mathbf{R}_{21} = \begin{bmatrix} \cos 2\theta & \sin 2\theta & 0 \\ -\sin 2\theta & \cos 2\theta & 0 \\ 0 & 0 & 1 \end{bmatrix}, \quad (1)$$

$$\mathbf{R}_{51} = \begin{bmatrix} \cos\omega & \sin\omega & 0 \\ -\sin\chi\sin\omega & \sin\chi\cos\omega & \cos\chi \\ \cos\chi\sin\omega & -\cos\chi\cos\omega & \sin\chi \end{bmatrix}, \quad (2)$$

and

$$\mathbf{R}_{35} = \begin{bmatrix} \cos\varphi & 0 & \sin\varphi \\ \sin\alpha_0\sin\varphi & \cos\alpha_0 & -\sin\alpha_0\cos\varphi \\ -\cos\alpha_0\sin\varphi & \sin\alpha_0 & \cos\alpha_0\cos\varphi \end{bmatrix}. \quad (3)$$

The rotation matrices can also be expressed in terms of the rotation and orientation matrices defined by Busing & Levy (1967) or those defined by Hamilton (1974*a*) if proper account is taken of the differences in definition of the diffractometer angles.

3.2. *Reflection and refraction operators*

In the diffraction process the incident beam can undergo three changes of direction: refraction at the air–crystal interface, reflection off the appropriate atomic planes and finally refraction at the crystal–air interface. The two processes may be represented by operators that act on the vectors representing the direction of the X-ray beam.

Denote the reflection operator acting about the plane normal to the principal axis Y_i in the frame $X_i Y_i Z_i$ by $\mathsf{R}_{D,Y}$. Being a linear transformation, it can be represented in matrix form as

$$\mathsf{R}_{D,Y} = \begin{bmatrix} 1 & 0 & 0 \\ 0 & -1 & 0 \\ 0 & 0 & 1 \end{bmatrix}. \quad (4)$$

The $X_i Z_i$ plane is parallel to the atomic planes.

Assume that there exists a refractive interface between the media k and l with normal parallel to the Y_i axis, and that the deviation of any X-ray passing through the interface is in accordance with Snell's law. The operator $\mathsf{R}_{R,Y}$, describing refraction through the interface, is then defined by

$$\mathsf{R}_{R,Y}\begin{bmatrix} x_i \\ y_i \\ z_i \end{bmatrix} = \begin{bmatrix} x_i(n_k/n_l) \\ \operatorname{sign}(y_i)\,|1 - (n_k/n_l)^2(1 - y_i^2)|^{1/2} \\ z_i(n_k/n_l) \end{bmatrix}, \quad (5)$$

where n_k and n_l are the refractive indices of the media k and l respectively. Equation (5) gives the unit direction vector representing the refracted ray in medium l in terms of the direction cosines (x_i,y_i,z_i) of the corresponding incident ray in medium k.

3.3. *The incident beam*

Since the extended-face crystal intercepts the entire incident beam, the dimensions of this beam must be well defined by collimators. We represent the incident beam by a cone of radiation with semi-angle γ_0 about the X_1 axis arising from an effective point source at $(-d,0,0)$ in the laboratory frame. The values of γ_0 and d may be calculated using the tube specifications and the geometry of the collimation system, or may be determined from photographs of the diffracted beam.

Each ray in the incident beam is described by the angles γ and η (Fig. 2), $(0 \le \eta < 180°, 0 \le \gamma \le \gamma_0)$ and contains all wavelengths. In the $X_1 Y_1 Z_1$ frame, the direction vector representing the ray (γ,η) is

$$\mathbf{s}_{0,1} = \begin{bmatrix} \cos\gamma \\ \cos\eta\sin\gamma \\ \sin\eta\sin\gamma \end{bmatrix}$$

and the parametric position vector describing the path traced by the ray is

$$\mathbf{T}_{0,1} = \mathbf{P}_{s,1} + r\mathbf{s}_{0,1} \quad (6)$$

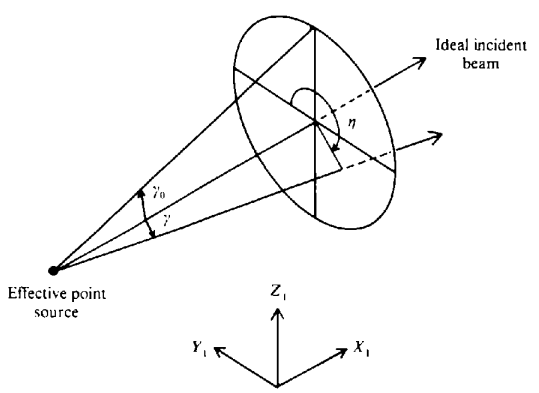

Fig. 2. The incident beam.

where r is the parameter and $\mathbf{P}_s$ is the position vector for the effective source:

$$\mathbf{P}_{s,1} = \begin{bmatrix} -d \\ 0 \\ 0 \end{bmatrix}.$$

The first subscript of the vectors $\mathbf{s}_{p,i}$, $\mathbf{P}_{p,i}$ and $\mathbf{T}_{p,i}$ denotes different vectors, the second indicates the frame of reference within which that vector is described. Hence $\mathbf{s}_{0,i}$ and $\mathbf{s}_{1,i}$ are two different vectors in the same frame of reference, while $\mathbf{s}_{0,i}$ and $\mathbf{s}_{0,j}$ are two different descriptions of the same vector. The scattering vector $\mathbf{S}_i$ and the crystal normal $\mathbf{n}_i$ have only the single subscript denoting the frame of reference.

3.4. *Intersection of the incident ray with the crystal surface*

The position vector $\mathbf{P}_{c,i}$ for the point of intersection of the incident ray (γ,η) with the crystal surface is given by the vector $\mathbf{T}_{0,i}$ that satisfies

$$\mathbf{T}_{0,i}.\mathbf{n}_i = 0. \tag{7}$$

From the definition of the $X_5 Y_5 Z_5$ frame, $\mathbf{n}_5$ is along the Y_5 axis. Equation (7) can be easily evaluated in the form $\mathbf{T}_{0,1}.\mathbf{R}'_{51}\,\mathbf{n}_5 = 0$ to give

$$\mathbf{P}_{c,1} = \begin{bmatrix} d(-1 + a\cos\gamma) \\ da\cos\eta\sin\gamma \\ da\sin\eta\sin\gamma \end{bmatrix}, \tag{8}$$

where

$$a = (\sin\chi\sin\omega)(\cos\gamma\sin\chi\sin\omega - \cos\eta\sin\gamma\sin\chi\cos\omega - \sin\eta\sin\gamma\cos\chi)^{-1}. \tag{9}$$

3.5. *The diffraction condition*

The internal incident ray in the $X_3 Y_3 Z_3$ coordinate system is parallel to $\mathbf{s}'_{0,3}$, where

$$\mathbf{s}'_{0,3} = \mathbf{R}_{35}\,\mathsf{R}_{R,Y}\,\mathbf{R}_{51}\,\mathbf{s}_{0,1}. \tag{10}$$

The prime denotes that the vector refers to a physical vector within the crystal. The unit vector $\boldsymbol{\tau}_i$, parallel to $\mathbf{S}_i$, is coincident with the Y_3 axis. Therefore, for diffraction to occur,

$$-\sin\theta'_B = \boldsymbol{\tau}_3.\mathbf{s}'_{0,3} = (\mathbf{s}'_{0,3})_Y, \tag{11}$$

where θ'_B is the Bragg angle within the crystal and is related to θ_B, the Bragg angle calculated from the wavelength in air, by

$$\sin\theta'_B = (\sin\theta_B)/n, \tag{12}$$

where n is the refractive index of the crystal. The subscripted parentheses in (11) denote the Y_3 component of $\mathbf{s}'_{0,3}$.

3.6. *The diffracted beam*

The specimen is assumed to be highly absorbing, so that all significant diffraction occurs only at the crystal surface. The diffracted beam then leaves the crystal at the same point at which it entered and we need only be concerned with the change in direction of the rays at each interface and interaction. The external diffracted ray $\mathbf{s}_{1,i}$ is obtained by applying the refraction and reflection operators to the external incident ray including, where necessary, the appropriate rotation transformations. In the $X_2 Y_2 Z_2$ frame the direction vector representing the external diffracted ray is therefore

$$\mathbf{s}_{1,2} = \mathbf{R}_{21}\,\mathbf{R}'_{51}\,\mathsf{R}_{R,Y}\,\mathbf{R}'_{35}\,\mathsf{R}_{D,Y}\,\mathbf{R}_{35}\,\mathsf{R}_{R,Y}\,\mathbf{R}_{51}\,\mathbf{s}_{0,1}. \tag{13}$$

The wavelength of this particular diffracted ray is determined by the diffraction condition satisfied by the incident ray.

The parametric vector equation of the path traced out by the external diffracted ray is

$$\mathbf{T}_{1,2} = \mathbf{R}_{21}\,\mathbf{P}_{c,1} + r\mathbf{s}_{1,2}. \tag{14}$$

At the detector face or aperture $(\mathbf{T}_{1,2})_X = t$. Solving (14) for r gives the point of intersection of the diffracted ray with the detector:

$$\mathbf{P}_{d,2} = \mathbf{R}_{21}\,\mathbf{P}_{c,1} + |t - (\mathbf{R}_{21}\,\mathbf{P}_{c,1})_X|\,\mathbf{s}_{1,2}/(\mathbf{s}_{1,2})_X. \tag{15}$$

In the following sections the above description will be applied to several specific situations encountered in extended-face crystal diffractometry. In the remainder of this paper assume that refraction can be ignored and hence that $\mathsf{R}_{R,Y}$ can be omitted. The effect of refraction on the optimum orientation of the crystal for reflection will be treated elsewhere (McIntyre, 1981).

For a given reflection, the crystal is correctly oriented when the external diffracted ray corresponding to the central incident ray ($\gamma = 0°$) lies along the X_2 axis. This does not, however, fix θ since ω and θ may then vary in the ratio 1:1 and still the central diffracted ray lies along the X_2 axis. The value of θ becomes fixed when a particular wavelength is chosen. To specify completely the orientation of the crystal and diffractometer when a reflection is so oriented, it is sufficient to quote the values of θ, α_0 and φ. The remaining angles, χ and ω, are then determined by the diffraction condition (7).

4. Experimental

All beam photographs presented in this paper were obtained using the extended-face specimen of InAs described in Appendix I. A Picker four-circle manual diffractometer with a 1·5 mm incident-beam collimator was used in conjunction with an Elliott Avionics type no. T × 12 fine-focus molybdenum X-ray tube. This combination of X-ray tube and collimating system gives effective point-source parameters of $d = 194$ mm

and $\gamma_0 = 0{\cdot}38°$. The collimator is larger than we would use for integrated intensity measurements, but was chosen to exhibit clearly the effects described. Ilford Industrial (G) X-ray film was used to photograph the diffracted beam.

5. The diffracted image in the asymmetric reflection position

The crystal is correctly oriented in the asymmetric reflection position for a given value of φ if

$$\chi = 90° - \tan^{-1}(\tan\alpha_0 \cos\varphi) \qquad (16a)$$

and

$$\omega = \theta + \sin^{-1}(\sin\alpha_0 \sin\varphi) \qquad (16b)$$

(Hamilton, 1974*b*). We also define

$$\varepsilon = \sin^{-1}(\sin\alpha_0 \sin\varphi) \qquad (17a)$$

and

$$\omega_B = \theta_B + \varepsilon. \qquad (17b)$$

The diffraction condition, obtained by evaluating (11) with the Euler angles from (16), is

$$-\sin\theta_B = -\sin\theta\cos\gamma + \cos\theta\cos\eta\sin\gamma. \qquad (18)$$

Note that (18) is independent of φ since rotation to a new φ value with the corresponding χ and ω settings from (16) leaves $\mathbf{S}_1$ unchanged in direction. When θ_B and θ are fixed, there are two solutions for η from (18) for each value of γ, corresponding to the incident ray (γ,η) being above or below the diffraction plane. In the diffraction plane the solutions of (18) are

$$\eta = 0° \quad \text{and} \quad \gamma = \theta - \theta_B, \quad \text{for } \theta > \theta_B, \qquad (19a)$$

and

$$\eta = 180° \quad \text{and} \quad \gamma = \theta_B - \theta, \quad \text{for } \theta < \theta_B. \qquad (19b)$$

The solutions for (γ,η) for the two $K\alpha$ components of the InAs 664 reflection are plotted in Fig. 3. The θ value was chosen to be the weighted average of the θ_B for the two $K\alpha$ components. As expected from the form of (18), the η *vs* γ curves are symmetric about the diffraction plane. At this small beam divergence the sections of the incident beam that give rise to diffraction for the two $K\alpha$ components are very nearly straight lines in the γ,η plane (parallel to the Y_1Z_1 plane) and perpendicular to the diffraction plane. Each wavelength in the continuum in a small interval about the $K\alpha$ components will also give rise to an η *vs* γ curve similar to those of the $K\alpha$ components. For each point within the circle $\gamma = \gamma_0$ of Fig. 3 the diffraction condition is satisfied by one wavelength. Thus for each ray in the incident beam cone defined by $\gamma = \gamma_0$, the crystal will select the appropriate wavelength to give Bragg diffraction.

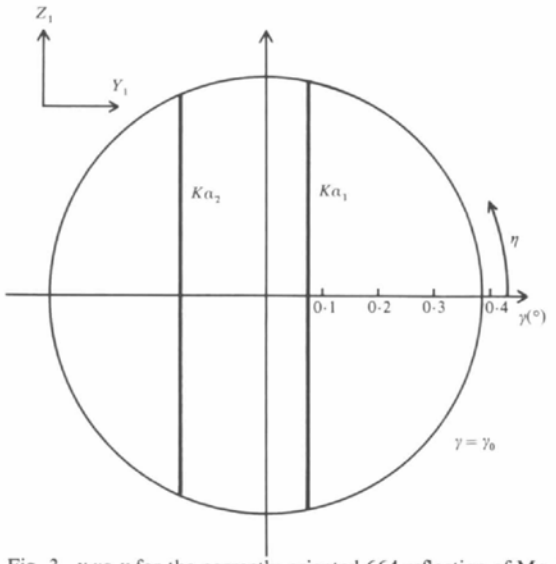

Fig. 3. γ *vs* η for the correctly oriented 664 reflection of Mo $K\alpha$ by InAs. $\theta_{K\alpha_1} = 33{\cdot}40°$, $\theta_{K\alpha_2} = 33{\cdot}63°$, $\alpha_0 = 25{\cdot}54°$.

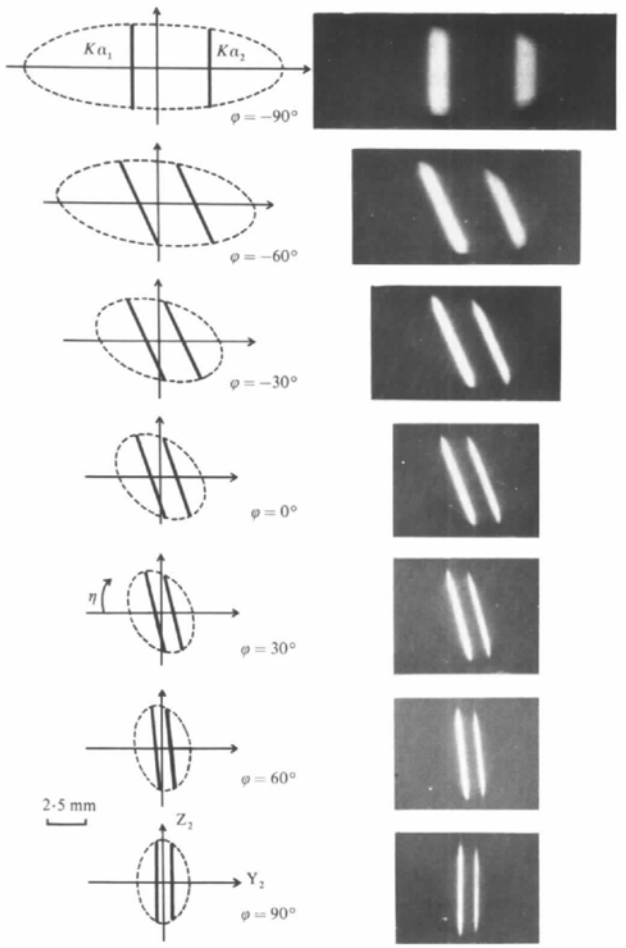

Fig. 4. Predicted and experimental diffracted-beam images for the 664 reflection of InAs for a range of values of φ. The origin and direction of increasing η around the perimeter is indicated on the image for $\varphi = 30°$. $\theta_{K\alpha_1} = 33{\cdot}40°$, $\theta_{K\alpha_2} = 33{\cdot}63°$, $\alpha_0 = 25{\cdot}54°$, $t = 218$ mm.

We find the corresponding diffracted image at the detector face by evaluating (15) for each of the two $K\alpha$ components using the (γ,η) values from (18), and for the envelope of the beam given by $\gamma = \gamma_0$. For each φ the diffracted image consists of two essentially straight lines for the $K\alpha$ components superimposed on an oval region corresponding to the continuous background. In general the $K\alpha$ images, and indeed the image for each wavelength in the continuum, are not perpendicular to the diffraction plane, due to the inclination of the crystal face to the diffraction plane. Fig. 4 presents the predicted and experimental diffracted images for a range of φ values for the InAs 664 reflection. The similarity between the predicted and experimental images shows the extent to which our assumptions are valid. The apparent double imaging of each component (seen more clearly in Fig. 5*c* and *d*) reflects the limitations of our approximation of the real source by an effective point source. The focusing and defocusing nature of the reflection from the extended-face crystal for respectively positive and negative values of ε is clearly evident in Fig. 4, both in the width of the total image and in the widths and separations of the characteristic line images.

Several useful expressions can be derived from (15). The inclination of the image of the wavelength component with Bragg angle θ_B, evaluated in the diffraction plane and for $\theta = \theta_B$, is (Appendix II)

$$\left(\frac{\mathrm{d}z_2}{\mathrm{d}y_2}\right)_{\gamma=0} = -(1 + t/d)\sin\omega_B \tan\chi/\sin 2\theta_B. \quad (20)$$

For most practical beam divergences, (20) can be considered to be valid for the entire θ range over which the component with Bragg angle θ_B diffracts. For a given reflection the inclination increases as t/d increases so that in the limit $t/d \to \infty$ the $K\alpha$ images are perpendicular to the diffraction plane. Both the inclination of the $K\alpha$ images and the skewness of the diffracted-beam envelope depend on φ as may be seen from the images of Fig. 4.

The Y_2 intercept of the image of the wavelength component with Bragg angle θ_B is (Appendix II)

$$y_{0,2} = -d\tan(\theta - \theta_B)\sin(\theta_B - \varepsilon)/\sin(\theta_B + \varepsilon) - t\tan(\theta - \theta_B). \quad (21)$$

From (21), the separation of the $K\alpha$ images parallel to the Y_2 axis is

$$\Delta y_2 = d[\tan(\theta_2 - \theta)\sin(\theta_2 - \varepsilon)/\sin(\theta_2 + \varepsilon) + \tan(\theta - \theta_1)\sin(\theta_1 - \varepsilon)/\sin(\theta_1 + \varepsilon)] + t[\tan(\theta_2 - \theta) + \tan(\theta - \theta_1)], \quad (22)$$

where θ_1 and θ_2 are the Bragg angles for the $K\alpha_1$ and $K\alpha_2$ components respectively.

We obtain an almost exact expression for the total height of the image from evaluation of $\mathrm{d}(\mathbf{P}_{d,2})_Z/\mathrm{d}\eta$ with $\gamma = \gamma_0$ (Appendix III):

$$h \simeq 2(d + t)\tan\gamma_0. \quad (23)$$

The maximum and minimum positions in the Z_2 direction correspond very closely to $\eta = \pm 90°$

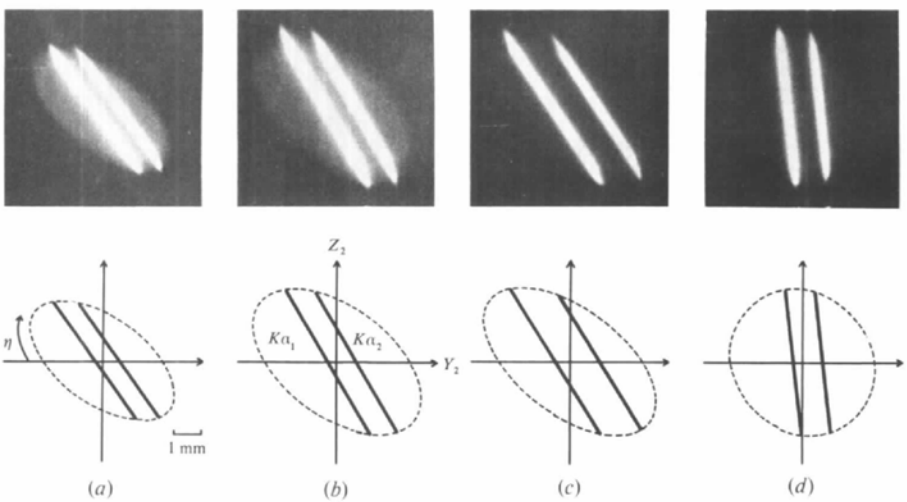

Fig. 5. Predicted and experimental diffracted-beam images of InAs reflections at the symmetric position ($\varphi = 0°$).

	$h\,k\,l$	θ (°)	α_0 (°)	t (mm)	Exposure (min)
(*a*)	4 4 4	24·04	34·56	141	5
(*b*)	4 4 4	24·04	34·56	218	5
(*c*)	6 4 6	33·48	40·09	218	10
(*d*)	5 5 1	24·83	7·43	218	7

Photographs (*a*) and (*b*) have been overexposed to emphasize the diffracted-beam envelope.

irrespective of the other parameters. Equation (23) is exact if $\alpha_0 = 0°$, or $\varphi = \pm 90°$.

From (19) and (21) the width of the image in the diffraction plane is

$$W_0 = d \tan \gamma_0 |\sin(\theta - \varepsilon + \gamma_0)/\sin(\theta + \varepsilon + \gamma_0) + \sin(\theta - \varepsilon - \gamma_0)/\sin(\theta + \varepsilon - \gamma_0)| + 2t \tan \gamma_0. \quad (24)$$

It is apparent from Fig. 4 that for reflections with $\alpha_0 \neq 0°$ and $\varphi \neq \pm 90°$ the total image width (the width of the projection onto the Y_2 axis) is greater than W_0 because of the skewness of the diffracted-beam envelope. The total image width is given by W_0 only when $\mathbf{n}_i$ lies in the diffraction plane (*i.e.* $\alpha_0 = 0°$ or $\varphi = \pm 90°$).

The total image width $W_{2\theta}$ is found from the maximum and minimum values of $(\mathbf{P}_{d,2})_Y$ with respect to η for $\gamma = \gamma_0$. These may be found numerically by trial and error or by Newton–Raphson iteration. Alternatively, an approximate but more convenient analytical solution, described in Appendix IV, gives

$$W_{2\theta} \simeq |W_0^2 + h^2/(\mathrm{d}z_2/\mathrm{d}y_2)^2_{\gamma=0}|^{1/2}. \quad (25)$$

As one moves away from the symmetric position, the difference between $W_{2\theta}$ and W_0 decreases until $\varphi = \pm 90°$, where $W_{2\theta} = W_0$ and $W_{2\theta}$ is a maximum/minimum. The increase of $W_{2\theta}$ near $\varphi = -90°$ (the deconcentrating position) is quite dramatic (Fig. 4). Note that W_0 consists of two contributions from the two intersections of the diffracted-beam envelope with the diffraction plane, $W_0^- = |y_{0,2}(\gamma_0, \eta = 0°)|$ and $W_0^+ = |y_{0,2}(\gamma_0, \eta = 180°)|$. Since W_0^- and W_0^+ are in general unequal the envelope is not spatially centred in the Y_2Z_2 plane when (16) is satisfied. The maximum value of $|y_{0,2}(\gamma_0, \eta)|$ over the full φ range for a given reflection occurs for $\varphi = -90°$, where $\varepsilon = -\alpha_0$ and $\eta = 0°$, and

$$y_{0,2} = -\tan \gamma_0 |t + d \sin(\theta + \alpha_0 - \gamma_0)/\sin(\theta - \alpha_0 - \gamma_0)|. \quad (26)$$

6. The diffracted image at the symmetric reflection position

Since the positions of symmetric reflection, where the ideal incident and diffracted beams make equal angles with the normal to the surface, are those normally used for routine data collection we present explicitly the equations describing the images obtained at these positions. In our geometry, the Euler angles to orient the crystal at the two positions of symmetric reflection are

$$A: \omega = \theta, \quad \chi = 90° - \alpha_0, \quad \varphi = 0°; \quad (27a)$$

and

$$B: \omega = \theta, \quad \chi = 90° + \alpha_0, \quad \varphi = 180°. \quad (27b)$$

Here we present only the results for A: the results for B are then obtained by reflection across the diffraction plane. The predicted and experimental images for the 444, 646 and 511 reflections at the symmetric position are given in Fig. 5.

The equations for the inclination, the Y_2 intercept, the component separation and the image width in the diffraction plane reduce to

$$(\mathrm{d}z_2/\mathrm{d}y_2)_{\gamma=0} = -(1 + t/d) \cot \alpha_0/2 \cos \theta_B, \quad (28)$$

$$y_{0,2} = -(d + t) \tan(\theta - \theta_B), \quad (29)$$

$$\Delta y_2 = (d + t)|\tan(\theta_2 - \theta) + \tan(\theta - \theta_1)|, \quad (30)$$

$$W_0 = 2(d + t) \tan \gamma_0. \quad (31)$$

Note that $y_{0,2}$ and Δy_2 are independent of α_0 and that W_0, in contrast to the asymmetric case, is even independent of the particular reflection (compare Fig. 5*b*, *c* and *d*). The image height is again given by (23) and the total image width (25), from (28) and (31), is

$$W_{2\theta} \simeq 2 \tan \gamma_0 |(d + t)^2 + 4d^2 \tan^2 \alpha_0 \cos^2 \theta_B|^{1/2}. \quad (32)$$

The increase in the image width with increasing α_0 is similar to the defocusing observed in the Schulz reflection technique for the determination of preferred orientation (Schulz, 1949; Huijser-Gerits & Rieck, 1974). If we choose a collimator to give an incident-beam cross section that is rectangular such that the two edges parallel to the Y_1 axis subtend an angle γ_0 at the source and those parallel to the Z_1 axis subtend an angle γ_1 at the source, the diffracted image at the symmetric position is a parallelogram with two edges parallel to the Y_2 axis and two edges inclined in the Y_2Z_2 plane with gradient given by (29). The total image width (the width of the projection onto the Y_2 axis) is

$$W_{2\theta} = 2(d + t) \tan \gamma_1 + 4d \tan \gamma_0 \tan \alpha_0 \cos \theta_B. \quad (33)$$

Since $d \tan \gamma_0$ is the width of the incident beam at the sample, the last term in (33) is identical to the expression obtained by Tenckhoff (1970) for the increased width of the image due to the tilt of the sample in the Schulz technique.

7. The optimum scanning ratio

In all types of scans currently used to measure the integrated intensity with a conventional four-circle diffractometer, the crystal is rotated about the ω axis through the reflecting position. The scanning range is identical in all cases and within our present assumptions the minimum limits of the scan are determined by the ω positions nearest to the peak maximum where neither characteristic wavelength of

the doublet can diffract. Since $\theta_2 > \theta_1$, (19) gives the upper and lower scan limits as, respectively,

$$\omega_u = \omega_2 + \gamma_0, \tag{34a}$$

$$\omega_l = \omega_1 - \gamma_0. \tag{34b}$$

The scan range is

$$\begin{aligned}\Delta\omega &= \omega_u - \omega_l = \omega_2 - \omega_1 + 2\gamma_0 \\ &= \theta_2 - \theta_1 + 2\gamma_0 = \Delta\theta_{1,2} + 2\gamma_0.\end{aligned} \tag{34c}$$

Obviously the total radiation diffracted by the crystal is the same in all cases.

The differences between the various types of scans are in the relative velocities of the detector and crystal and in the sizes of the receiving apertures. The theoretical minimum dimensions of the aperture are determined by two criteria: (1) The detector must receive completely both $K\alpha$ images over the full range of the peak scan; (2) The background correction must measure the continuous radiation within the diffracted-beam envelope in a manner consistent with the peak scan. Since the scattering vectors for all reflections in the same central lattice-row line are parallel, the diffracted-beam envelopes of all these reflections are exactly superimposed. In addition to the spectrum of the reflection being studied, the total intensity scattered into the diffracted-beam envelope will contain significant contributions from the background spectra of neighbouring reflections in the same central lattice-row line. This is discussed in greater detail by Alexander & Smith (1962) and Burbank (1964). The background correction must therefore remove systematically all wavelengths other than the $K\alpha$ doublet, *i.e.* all the Bragg-scattered background. We assume that both the Bragg and incoherent backgrounds (excluding thermal diffuse scattering which can be calculated) vary linearly with ω within $\Delta\omega$ and with θ within the 2θ range covered by the detector during the scan.

The images of Figs. 4 and 5 correspond to stationary-crystal–stationary-detector measurements. During a scan the characteristic line images move across the diffracted beam within the perimeter $\gamma = \gamma_0$ and parallel to the Y_2 axis. In general the diffracted-beam envelope itself also moves parallel to the Y_2 axis with a velocity dependent on the coupling between ω and θ. Therefore, the image height, $2(d + t)\tan\gamma_0$, constant for a particular choice of diffractometer and collimator, is also the minimum receiving aperture height for all scan modes using equatorial geometry.

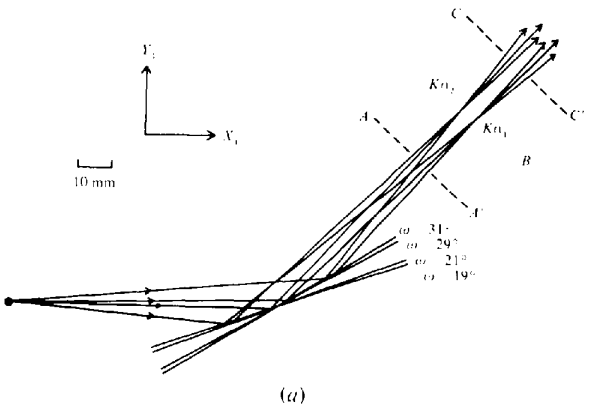

(*a*)

Fig. 6. A scan at the symmetric position. Here $d = 80$ mm, $t_A = 60$ mm, $t_B = 80$ mm, $t_C = 100$ mm, $\gamma_0 = 5°$, $\theta_1 = 24°$, $\theta_2 = 26°$ and $\alpha_0 = 40°$. Therefore, the $K\alpha_1$ component is diffracted in the range $19 < \omega \leq 29°$, and the $K\alpha_2$ component is diffracted in the range $21 \leq \omega \leq 31°$. (*a*) Cross section in the diffraction plane. The crystal surface and the incident and diffracted rays for the $K\alpha_1$ component are shown for $\omega = 19$ and 29°; those for the $K\alpha_2$ component are shown for $\omega = 21$ and 31°. The rays for both components at $\omega = 25°$ are also shown. As ω increases, the image of each component moves away from A towards A', remains stationary at B, and moves away from C' towards C. For $t < t_B$, $W'_{\omega 0}$ is defined by the diffracted beams for the $K\alpha_2$ component at $\omega = 21°$ and the $K\alpha_1$ component at $\omega = 29°$; for $t > t_B$ by the diffracted beams for the $K\alpha_1$ component at $\omega = 19°$ and the $K\alpha_2$ component at $\omega = 31°$. (*b*) The diffracted images at AA' during an ω scan. The diffracted-beam envelope moves along Y_2 while the Y_2Z_2 plane remains stationary in the $X_1Y_1Z_1$ frame. The receiving aperture widths for various scan modes are indicated. (*c*) The diffracted images at CC' during an ω:2θ scan. The diffracted-beam envelope is stationary in the Y_2Z_2 plane while the $X_2Y_2Z_2$ frame rotates around Z_1. The inclined aperture with width $W'_{\omega 0}$ appropriate to an ω scan is also shown.

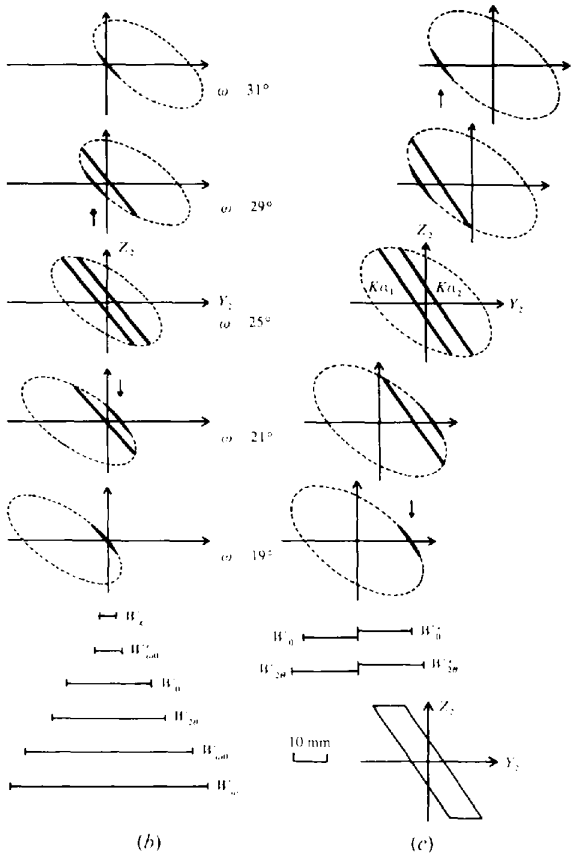

(*b*) (*c*)

In $\omega:2\theta$ scans where the motions of the crystal and detector are coupled in the ratio 1:2, the envelope remains stationary in the $X_2 Y_2 Z_2$ frame except for the slight variation in shape with θ. The motion of the $K\alpha$ images in this case is shown schematically in Fig. 6(*c*). For $\omega:2\theta$ scans, therefore, the width of the envelope in the $X_2 = t$ plane also gives the minimum width of the receiving aperture that satisfies the first criterion. The Bragg-scattered background can be subtracted by using stationary-background measurements at the scan limits to satisfy the second criterion. If the aperture is rectangular with sides perpendicular to the diffraction plane, then $W_{2\theta}$ is the minimum aperture width for each reflection and consists of the two generally unequal contributions, $W^+_{2\theta}$ and $W^-_{2\theta}$ (see Fig. 6*c*). The expression for $W_{2\theta}$, (25), or (32) if at the symmetric reflection position, can be used to determine for which reflections all of the diffracted-beam envelope is received by the detector if γ_0, d, t and the receiving aperture width W_A are fixed, or to determine the minimum values for W_A or the maximum for γ_0 to detect completely a particular reflection. If γ_0 can be altered it is usually convenient to set it such that $W_{2\theta}$ for each reflection that is to be measured in the data collection is significantly smaller than W_A to allow some tolerance in the setting angles of each reflection. In the case of measurements of asymmetric reflections over the full φ range (see, for example, Mathieson, 1975, 1977), Fig. 4 emphasizes that the diffractometer geometry must be well known to ensure that all the diffracted beam is detected.

In the case of ω scans, if we wish to subtract the Bragg scattering due to non-characteristic wavelengths by using stationary background counts at the scan limits, the correct minimum aperture is that which receives the complete diffracted-beam envelope during the scan $\Delta\omega$. In contrast to $\omega:2\theta$ scans, the scan range and the aperture width are closely interrelated. With reference to Figs. 6(*b*) and 7 the minimum aperture width is

$$W_\omega = 2t\tan(\Delta\omega) + [W^+_{2\theta}(\omega_u) + W^-_{2\theta}(\omega_l)]/\cos^2(\Delta\omega). \tag{35}$$

The orientation of the detector aperture is given by $\theta = \theta_{1,2} = (\theta_1 + \theta_2)/2$.

For both the $\omega:2\theta$ and ω scans described above, the area of the receiving aperture can be decreased and still the complete diffracted-beam envelope is accepted, if we relax the assumption of a rectangular aperture perpendicular to the diffraction plane and instead employ an aperture whose edges describe a parallelogram. The horizontal edges are separated by h; the other two edges are inclined in the $Y_2 Z_2$ plane with gradient $(dz_2/dy_2)_{y=0}$. For $\omega:2\theta$ scans, the minimum horizontal width is then W_0 and for measurements at the symmetric position is independent of the reflection [see (31)]. For ω scans the minimum width is

$$W_{\omega 0} = 2t\tan(\Delta\omega) + [W^+_0(\omega_u) + W^-_0(\omega_l)]/\cos^2(\Delta\omega). \tag{36}$$

Although it remains to be seen whether it is feasible to use such an inclined aperture in practice, we shall assume that one is available in the following derivations of aperture dimensions for the ω scan and for the optimum scan mode.

What is the smallest inclined-aperture width for ω scans that will satisfy the first criterion? The smallest aperture is defined by the length along the Y_2 axis traced out during the scan by the $K\alpha_1$ and $K\alpha_2$ images when θ is set at $\theta_{1,2}$. Since both the diffracted-beam envelope and the $K\alpha$ images rotate around Z_1 at nearly constant (but not equal) velocities, the limits of this length correspond to the ω positions at which the $K\alpha$ components first begin or first cease to diffract. There are two possibilities:

(*a*) If the $K\alpha$ images move towards negative Y_2 as ω increases, the aperture width is (Fig. 6*b*)

$$W'_{\omega 0} = [W^-_0(\omega_1 + \gamma_0) + W^+_0(\omega_2 - \gamma_0)]/\cos^2(2\gamma_0 - \Delta\theta_{1,2}) - 2t\tan(2\gamma_0 - \Delta\theta_{1,2}). \tag{37}$$

(*b*) If the $K\alpha$ images move towards positive Y_2 as ω increases, the aperture width is (Fig. 6*c*)

$$W'_{\omega 0} = 2t\tan(\Delta\omega) - [W^-_0(\omega_u) + W^+_0(\omega_l)]/\cos^2(\Delta\omega). \tag{38}$$

For a given diffractometer and reflection the larger of these is the correct expression for the minimum width. If they are equal then the $K\alpha$ images remain stationary in the $X_1 Y_1 Z_1$ frame. At each point during the peak scan, usually only a fraction of the diffracted-beam envelope is accepted by the detector aperture. Obviously stationary counts cannot sample the Bragg-scattered background within the envelope in the same manner as the peak scan and therefore cannot be used to obtain a background correction.

However, in both cases a background correction consistent with the peak scan can be obtained from two

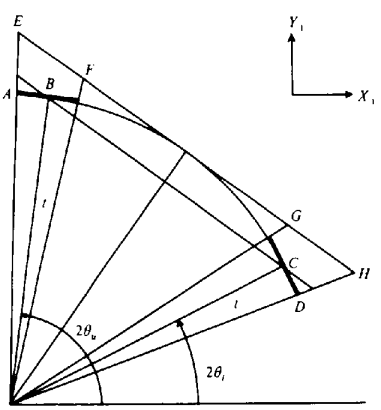

Fig. 7. Geometry for determining the aperture width for ω scans. Cross section in the diffraction plane. $AB = W^+_0(\omega_u)$, $CD = W^-_0(\omega_l)$, $BC = 2t\sin(\Delta\omega)$, $EH = W_{\omega 0}$, $FG = W'_{\omega 0}$, case (*a*).

additional ω scans, the first from $\omega_l - \Delta\omega$ to ω_l with $\theta = \theta_{1,2} - \Delta\omega$, the second from ω_u to $\omega_u + \Delta\omega$ with $\theta = \theta_{1,2} + \Delta\omega$. The aperture width in both background scans is $W'_{\omega 0}$. In case (*a*), the diffracted-beam envelope passes only partially across the detector aperture, but in an identical manner in each of the three scans so that the area of the envelope cross section seen in each pass is the same. In the peak scan the $K\alpha$ images move across the aperture within the envelope in opposite direction to the motion of the envelope. In case (*b*), the diffracted-beam envelope passes completely across the aperture in each of the three scans and in the peak scan the $K\alpha$ images move across the aperture in the same direction as, but slower than, the envelope.

Whenever the background is to be determined by stationary measurements at the scan limits the $\omega{:}2\theta$ scan requires a smaller aperture than the ω scan. Often the $\omega{:}2\theta$ scan will be the only possible choice, particularly for asymmetric reflections where W_0 is comparable with the width of the detector face. We note that in this regard the step scan favoured in automatic data collections is equivalent to the continuous scan with stationary background measurements.

Any type of scan involving another ratio for the coupling between the crystal and detector motions is only worth considering if it provides an improvement in the peak-to-background ratio. Werner (1972) has derived the coupling ratio necessary to keep the centroid of the two $K\alpha$ components in the diffracted beam aligned with the centre-line of the detector. This allows one to use the minimum possible detector-aperture width determined only by the separation of the $K\alpha$ components, thus keeping the background contribution to the scan as low as possible. Werner considered both single crystals that are small compared with the X-ray source and large crystals where the shift, as the crystal is rotated, of the centre of scattering relative to the centre of the instrument is important. Einstein (1974) and Denne (1977*b*) have also derived expressions for the optimum coupling ratio for X-ray measurements. Denote the optimum coupling ratio between the crystal and detector rotations (*i.e.* between ω and 2θ) by g; the corresponding scan is an $\omega{:}g\theta$ scan.

We shall now derive the optimum scanning ratio for asymmetric reflection from an extended-face crystal. Within our assumptions the dominant cause of the difference in g from 1, the value for the idealized conditions of a centred point specimen and a monoenergetic source (Werner, 1972; Denne, 1977*b*), is the finite size of the crystal face. Assume that the crystal and detector are initially oriented to maximize the intensity for a reflection with a Bragg angle of θ_B and an arbitrary value of φ. The values of χ and ε are then fixed by (16). At the optimum orientation, $\omega = \omega_B = \theta_B + \varepsilon$.

Now allow ω to vary. The ray that has diffracted with a Bragg angle of θ_B and lies in the diffraction plane is given by

$$\mathbf{T}_{1,1} = \mathbf{P}_{c,1} + r\mathbf{s}_{1,1} \tag{39}$$

[compare with (14)] evaluated for $\eta = 0°$ and $\gamma = \omega - \omega_B$. The detector lies a distance t from the centre of the instrument. From the constraint

$$(\mathbf{T}_{1,1})_X^2 + (\mathbf{T}_{1,1})_Y^2 = t^2, \tag{40}$$

r in (39) is found to give $\mathbf{P}_{d,1}$, the point of intersection of the diffracted ray with the detector [compare with (15)]. Denote this value of r by r_d. The detector is to be aligned such that the tip of $\mathbf{P}_{d,1}$ touches the X_2 axis at t. This condition determines 2θ, thus

$$2\theta = \tan^{-1}|(\mathbf{P}_{d,1})_Y/(\mathbf{P}_{d,1})_X|. \tag{41}$$

The optimum scanning ratio is

$$g = \mathrm{d}2\theta/\mathrm{d}\omega = |(\mathbf{P}_{d,1})_X\,\mathrm{d}(\mathbf{P}_{d,1})_Y/\mathrm{d}\omega - (\mathbf{P}_{d,1})_Y\mathrm{d}(\mathbf{P}_{d,1})_X/\mathrm{d}\omega|/t^2, \tag{42}$$

where the derivatives are, from (39),

$$\mathrm{d}\mathbf{P}_{d,1}/\mathrm{d}\omega = \mathrm{d}\mathbf{P}_{c,1}/\mathrm{d}\omega + (\mathrm{d}r_d/\mathrm{d}\omega)\mathbf{s}_{1,1} + r_d\,\mathrm{d}\mathbf{s}_{1,1}/\mathrm{d}\omega. \tag{43}$$

To find r_d and g we also need a simple expression for $\mathbf{s}_{1,1}$. Let us assume for the moment that the ω and θ axes are coupled in the ratio 1:1, so that $\theta = \theta_B + \omega - \omega_B$. The incident ray that lies in the diffraction plane and satisfies the diffraction condition is

$$\mathbf{s}_{0,1} = \begin{bmatrix} \cos(\omega - \omega_B) \\ \sin(\omega - \omega_B) \\ 0 \end{bmatrix}.$$

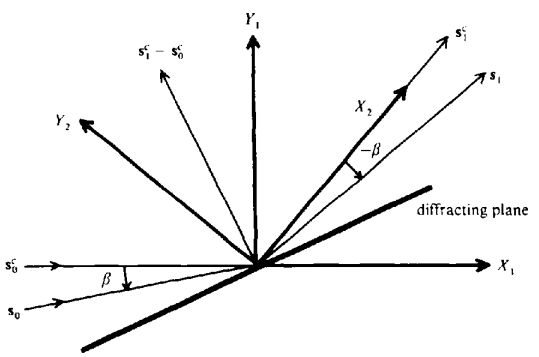

Fig. 8. Projection onto the $X_1 Y_1$ plane. The specimen is aligned so that $\mathbf{s}_0^c$ may diffract; the scattering vector is then $\mathbf{s}_1^c - \mathbf{s}_0^c$. If a ray $\mathbf{s}_0$ at an angle β to $\mathbf{s}_0^c$ also diffracts, the corresponding diffracted ray is at an angle $-\beta$ to $\mathbf{s}_1^c$. X_2 is parallel to $\mathbf{s}_1^c$. Then, if the direction cosines of $\mathbf{s}_0$ in the $X_1 Y_1 Z_1$ frame are (a,b,c), the direction cosines of $\mathbf{s}_1$ in the $X_2 Y_2 Z_2$ frame are $(a,-b,c)$.

The corresponding diffracted ray in the $X_2 Y_2 Z_2$ frame is then

$$\mathbf{s}_{1,2} = \begin{bmatrix} \cos(\omega - \omega_B) \\ -\sin(\omega - \omega_B) \\ 0 \end{bmatrix},$$

by the argument presented in the caption to Fig. 8. In the laboratory frame the diffracted ray is

$$\mathbf{s}_{1,1} = \mathbf{R}'_{21}\,\mathbf{s}_{1,2} = \begin{bmatrix} \cos(2\theta_B + \omega - \omega_B) \\ \sin(2\theta_B + \omega - \omega_B) \\ 0 \end{bmatrix}. \quad (44)$$

Relax the assumption of 1:1 coupling between ω and θ. Equations (40) and (42) then yield the general expression for g:

$$\begin{aligned} g = (1/t^2)\{&r_d^2 + d^2|\sin^2\omega/\sin^2\omega_B \\ &- \sin(2\omega - \omega_B)/\sin\omega_B| \\ &+ r_d d|\sin\omega\cos 2\theta_B/\sin\omega_B - \sin(2\theta_B - \omega)/\sin\omega_B \\ &- \cos(2\theta_B + \omega - \omega_B)| \\ &+ (\mathrm{d}r_d/\mathrm{d}\omega)d|\sin\omega\sin 2\theta_B/\sin\omega_B \\ &- \sin(2\theta_B + \omega - \omega_B)|\}, \end{aligned} \quad (45)$$

where

$$\begin{aligned} r_d = d|&\cos(2\theta_B + \omega - \omega_B) - \sin\omega\cos 2\theta_B/\sin\omega_B| \\ &+ \{d^2|\cos^2(2\theta_B + \omega - \omega_B) \\ &- 2\sin\omega\cos 2\theta_B\cos(2\theta_B + \omega - \omega_B)/\sin\omega_B \\ &+ 2\sin\omega\cos(\omega - \omega_B)/\sin\omega_B \\ &- \sin^2\omega\sin^2 2\theta_B/\sin^2\omega_B - 1| + t^2\}^{1/2}, \end{aligned} \quad (46)$$

and

$$\begin{aligned} \mathrm{d}r_d/\mathrm{d}\omega = -\{&r_d d|\cos\omega\cos 2\theta_B/\sin\omega_B \\ &+ \sin(2\theta_B + \omega - \omega_B)| \\ &+ d^2|\sin\omega\cos\omega/\sin^2\omega_B \\ &- \cos(2\omega - \omega_B)/\sin\omega_B|\} \\ &\times \{r_d + d|\sin\omega\cos 2\theta_B/\sin\omega_B \\ &- \cos(2\theta_B + \omega - \omega_B)|\}^{-1}. \end{aligned} \quad (47)$$

At $\omega = \omega_B$, $r_d = t$ and we obtain

$$\begin{aligned} g &= |1 - (d/t)\sin(2\theta_B - \omega_B)/\sin\omega_B| \\ &= |1 - (d/t)\sin(\theta_B - \varepsilon)/\sin(\theta_B + \varepsilon)|. \end{aligned} \quad (48)$$

For the $K\alpha$ doublet we can use $\theta_B = \theta_{1,2}$ in (48). The corresponding aperture width in the diffraction plane, W_g, is given by Δy_2 from (22). Since $\Delta\theta_{1,2}$ is small, this simplifies to

$$W_g \simeq \Delta\theta_{1,2}|d\sin(\theta_{1,2} - \varepsilon)/\sin(\theta_{1,2} + \varepsilon) + t|, \quad (49)$$

where $\Delta\theta_{1,2}$ is in radians.

A comparison of the values for g calculated using (45) and (48) indicated that for our experimental arrangement the difference is less than 1% at the limits of the scan. The difference at the scan limits results from the ω dependence of g in (45): equation (48) is of course independent of ω. The exact expression for W_g is also ω dependent and the minimum aperture width occurs for $\omega = \omega_{1,2}$; however, the increase over the length of the scan is negligible. In practice, the ω dependence of g and W_g may be compensated for by a slight increase in W_g over its value from (49). Obviously the use of constant values for g and W_g will introduce a slight systematic error.

In the symmetric mode $g = 1 - d/t$ and the optimum coupling between the detector and the crystal is always less than 1. In fact, in the common case of equal source-to-crystal and crystal-to-detector distances, the optimum scan is an ω scan (Fig. 6*a*). That for $d > t$ the detector should be rotated in a direction opposite to the crystal motion results from the translation of the $K\alpha$ diffracting regions across the crystal surface as ω increases (Fig. 6*b*).

At the limits of the $\omega : g\theta$ scan only a fraction of the diffracted-beam envelope passes through the inclined receiving aperture. A background correction that also removes the non-characteristic Bragg scattering within the bandpass can be obtained from two additional $\omega : g\theta$ scans, the first from $\omega = \omega_l - \Delta\theta_{1,2}$ to $\omega = \omega_l - \Delta\theta_{1,2} + \Delta\omega$ with $\theta = \omega_l - \Delta\theta_{1,2} + \frac{1}{2}\Delta\omega$ at the centre of the scan, and the second from $\omega = \omega_u + \Delta\theta_{1,2} - \Delta\omega$ to $\omega = \omega_u + \Delta\theta_{1,2}$ with $\theta = \omega_u + \Delta\theta_{1,2} - \frac{1}{2}\Delta\omega$ at the centre of the scan. All scans have a bandpass of $\Delta\lambda_{1,2}$, the $K\alpha$ doublet splitting, and the bandpasses of the background scans are displaced by $\pm\Delta\lambda_{1,2}$ relative to the peak bandpass. In each scan the receiving aperture samples the diffracted-beam envelope in an identical manner.

Adoption of the $\omega : g\theta$ scan may be advantageous at low Bragg angles. A disadvantage of the extended-face technique is that unless the incident beam is severely collimated, there is a large range of angles between the incident rays and any particular scattering vector for a given setting of the diffractometer. For crystals with large unit cells this can lead to resolution problems. At low Bragg angles where $\Delta\theta_{1,2} < 2\gamma_0$ and thence $W_g < W_0$, the use of the $\omega : g\theta$ scan with an inclined aperture will minimize the range of angles in the incident beam eventually accepted by the detector and hence improve the resolution.

At higher Bragg angles where $\Delta\theta_{1,2} > 2\gamma_0$, the $\omega : 2\theta$ scan with inclined aperture is recommended, since $W_0 < W_g$ for each reflection. Both types of scans can have resolution problems. Since the diffracted-beam envelope for the particular scattering vector being considered remains stationary in the detector aperture for $\omega : 2\theta$ scans, the resolution is limited by neighbouring reflections in the central lattice-row line. For $\omega : g\theta$

scans the envelope passes across the detector aperture and the resolution is limited by the diffracted-beam envelopes of adjacent reflections in the equatorial plane. The smaller aperture area for the $\omega:2\theta$ scan compared to the $\omega:g\theta$ scan means that the incoherent contribution to the background is smaller, although the Bragg-scattered contribution is larger.

For a series of measurements over a wide range in θ, a combination of the two methods, $\omega:g\theta$ scans with background scans for $\Delta\theta_{1,2} < 2\gamma_0$, and $\omega:2\theta$ scans with stationary background counts for $\Delta\theta_{1,2} > 2\gamma_0$, both with inclined apertures, may be advantageous. The two scan modes are compatible provided the background measurements have been obtained correctly.

8. Discussion

What are the effects of finite intrinsic diffraction profiles, mosaic spread, absorption, source size and width of the characteristic X-ray lines? All five factors broaden the image for a particular wavelength and the diffracted-beam envelope, while all except absorption increase the minimum scan range. Corrections to $\Delta\omega$ and the aperture widths due to the mosaic spread, the finite source size and the natural dispersion of the spectral line found for small crystals (Alexander & Smith, 1962; Burbank, 1964; Ladell & Spielberg, 1966) may be similarly derived for extended-face crystals. Dispersion is most difficult to allow for because of the indefinite width of the Cauchy-like spectral-line profile (Ladell, Parrish & Taylor, 1959). In practice γ_λ, the correction to $\Delta\omega$, is often chosen to be a fixed multiple of the widths at half maximum intensity of the $K\alpha_1$ and $K\alpha_2$ lines, or to be defined by a balanced-filter pair, so that the scan includes a fixed percentage of the area under the calculated Cauchy distribution of the doublet (Burbank, 1964). If we include the mosaic spread γ_m, and the angle subtended by the source at the crystal γ_x, the corrected scan range is

$$\Delta\omega_c = \Delta\omega + \gamma_\lambda + \gamma_m + \gamma_x. \tag{50}$$

Spectral dispersion must be allowed for in the aperture widths for ω and $\omega:g\theta$ scans, while for $\omega:2\theta$ scans this is achieved purely by the increased scan range. The area swept out parallel to the $X_1 Y_1$ plane during the scan by the diffracted image for a particular wavelength is independent of γ_m, although the width of this image at any one point during the scan will be increased by the mosaic spread. Therefore $W'_{\omega 0}$ need not include a correction for γ_m but W_g must. For $\omega:2\theta$ scans and ω scans using stationary background counts the aperture widths must include terms in γ_m, since the diffracted-beam envelope is broadened by γ_m.

The corrected image and aperture widths are then

$$W_{0c} = W_0 + (2\gamma_m + \gamma_x + \gamma_a)t \tag{51}$$

$$W_{2\theta c} = W_{2\theta} + (2\gamma_m + \gamma_x + \gamma_a)t \tag{52}$$

$$W_{\omega c} = W_\omega + (2\gamma_m + \gamma_x + 2\gamma_\lambda + \gamma_a)t/\cos^2(\Delta\omega_c) \tag{53}$$

$$W_{\omega 0c} = W_{\omega 0} + (2\gamma_m + \gamma_x + 2\gamma_\lambda + \gamma_a)t/\cos^2(\Delta\omega_c) \tag{54}$$

$$W'_{\omega 0c} = W'_{\omega 0} + (\gamma_x + 2\gamma_\lambda + \gamma_a)t/\cos^2(\Delta\omega_c) \tag{55}$$

$$W_{gc} = W_g + (\gamma_m + \gamma_x + 2\gamma_\lambda + \gamma_a)t \tag{56}$$

and the corrected image height is

$$h_c = h + (2\gamma_m \sin\theta + \gamma_x)t, \tag{57}$$

where γ_m, γ_x, γ_α and γ_λ are in radians. To collect all diffracted rays that are attenuated less than $100p\%$, the correction due to absorption is

$$\gamma_a t = -\log_e(1-p)\sin(2\theta-\omega)\cos\theta/\mu\cos(\omega-\theta) \tag{58}$$

(McIntyre, 1981), where μ is the absorption coefficient, whose inverse is expressed in the same units as the aperture widths. Finite absorption shifts the centre of scattering in the positive X_1 direction. Rather than increasing the crystal height so that the centre of scattering coincides with the centre of the instrument, it is more practical to compensate for the shift by decreasing the 2θ setting at the start of the scans by the amount $\gamma_a/2$.

In this paper it is assumed that it is desirable to detect the complete $K\alpha$ doublet. Denne (1977*a*,*b*) has proposed a monochromation technique for accurate integrated-intensity measurements where small and reasonably perfect single crystals are used. His method employs restricted detector slits and the optimum scanning ratio appropriate to such crystals ($g = 1$) to select and maintain a given bandpass. The bandpass is not necessarily chosen to be the complete $K\alpha$ doublet. This monochromation technique could also be applied to measurements using extended-face specimens if the inclined aperture $\omega:g\theta$ scan is employed.

In the author's opinion the improvement in precision due to the increase in the peak-to-background ratio gained by using the inclined aperture $\omega:g\theta$ scan would be outweighed by an overall decrease in accuracy. While a limited bandpass is theoretically desirable, the practical difficulties of achieving and maintaining the very precise alignment required both of the crystal and of the aperture, particularly in measurements where the diffractometer angles are not optimized for all reflections (*e.g.* in automatic data collections), oppose the routine use of the inclined aperture $\omega:g\theta$ scan. It would be better to overcome the resolution problems by improving the collimation of the incident beam. Profile fitting may yield an alternative solution to that of Denne (1977*b*) to avoid systematic errors incurred by not collecting the complete profiles of the characteristic Bragg scattering.

The three-dimensional nature of diffraction from extended-face crystals encouraged development of the real-space description presented in this paper. The description has proved to be particularly suitable for investigating the geometric conditions imposed by the experimental hardware (collimators, apertures, *etc.*), the practicabilities of different scan modes and the effects of refraction (McIntyre, 1981). For other aspects of the experiment or for experimental arrangements different to ours, a reciprocal-space representation or a transformed reciprocal-space representation like that of Einstein (1974) may be more appropriate. The present discussion has been confined to equatorial-plane diffractometers. Similar methods with the appropriate definitions of instrument angles and frames of reference could be used to describe the real-space geometry of reflections from extended-face crystals using other instruments, for example inclination diffractometers or back-reflection Laue cameras.

I am indebted to Dr Z. Barnea for his continual encouragement and guidance throughout the course of this study. I am grateful to Mr D. Wentworth for his technical assistance and to Mr M. Brown for his photographic advice and for producing the prints of the diffracted-beam images. I also thank Miss Eleanor Rose, Department of Physics, University of Edinburgh for generously preparing the typescript. I gratefully acknowledge the financial support of a Commonwealth Postgraduate Research Award. The work has been supported by the Australian Research Grants Committee.

APPENDIX I
Preparation of the extended-face specimen of InAs

A single crystal of InAs, oriented from its cleavage habit, was cut parallel to the (011) cleavage planes using an abrasive wire saw. The cut face was ground with SiC abrasive of decreasing coarseness (particle size 70–28 μm) on a rotating steel grinding wheel, and then the ground face was successively polished with 302, 303 and 303½ Al_2O_3 (particle size 22–12 μm) on a flat steel surface. In both the above stages of polishing, water was used as a lubricant. The polishing process was continued using 304 Al_2O_3 (particle size 8 μm) embedded in a sheet of paper placed on a flat glass surface; the lubricant was CH_3OH. The process was found to be most effective when small concentrations of the etchant Br_2 (Sharma, 1966) were also added to the lubricant. To avoid selective etching, the concentration was less than 0·5% Br_2 in CH_3OH. Finally, the surface was successively polished with 0·3 μm α-Al_2O_3 and 0·05 μm γ-Al_2O_3 on a polishing cloth. Initially, distilled water was used as a lubricant and then the etchant solution.

The polished 24 × 16 mm face had a mirror finish and was parallel to the (011) plane to within 1·5°.

APPENDIX II
Inclination and separation of the characteristic line images

(i) *Inclination*

We assume that the crystal is correctly oriented in an asymmetric position [see (16)]. The scattering vector **S** then lies in the diffraction plane at an angle $(90° + \theta)$ to the X_1 axis. Furthermore, the central diffracted ray $\mathbf{s}_1^c$, corresponding to the central incident ray $\mathbf{s}_0^c$ ($\gamma = 0$), lies along the X_2 axis.

The direction cosines of a general diffracted ray (neglecting refraction) are given by

$$\mathbf{s}_{1,2} = \mathbf{R}_{21}\,\mathbf{R}_{51}^{t}\,\mathbf{R}_{35}^{t}\,\mathsf{R}_{D,Y}\,\mathbf{R}_{35}\,\mathbf{R}_{51}\,\mathbf{s}_{0,1}, \tag{59}$$

with

$$\mathbf{s}_{0,1} = \begin{bmatrix} \cos\gamma \\ \cos\eta\sin\gamma \\ \sin\eta\sin\gamma \end{bmatrix}. \tag{60}$$

Since **S** lies in the diffraction plane, the Z_1 component of this ray is unchanged during diffraction. From Fig. 8, the projection onto the $X_1\,Y_1$ plane, it is obvious that

$$\mathbf{s}_{1,2} = \begin{bmatrix} \cos\gamma \\ -\cos\eta\sin\gamma \\ \sin\eta\sin\gamma \end{bmatrix}. \tag{61}$$

Hence when χ and ω are given by (16)

$$\mathbf{R}_{21}\,\mathbf{R}_{51}^{t}\,\mathbf{R}_{35}^{t}\,\mathsf{R}_{D,Y}\,\mathbf{R}_{35}\,\mathbf{R}_{51} = \begin{bmatrix} 1 & 0 & 0 \\ 0 & -1 & 0 \\ 0 & 0 & 1 \end{bmatrix}. \tag{62}$$

The Y_2 and Z_2 components of (15) become

$$(\mathbf{P}_{d,2})_Y = (\mathbf{P}_{c,2})_Y - \cos\eta\sin\gamma[t - (\mathbf{P}_{c,2})_X]/\cos\gamma \tag{63a}$$

and

$$(\mathbf{P}_{d,2})_Z = (\mathbf{P}_{c,2})_Z + \sin\eta\sin\gamma[t - (\mathbf{P}_{c,2})_X]/\cos\gamma. \tag{63b}$$

The vectors $\mathbf{P}_{c,2}$ and $\mathbf{P}_{d,2}$ are functions of both η and γ. For a particular wavelength η is also a function of γ from (18) and $(\mathbf{P}_{d,2})_Y$ and $(\mathbf{P}_{d,2})_Z$ become y_2 and z_2 respectively. The inclination of the characteristic line image at the detector is then

$$\mathrm{d}z_2/\mathrm{d}y_2 = (\mathrm{d}z_2/\mathrm{d}\gamma)/(\mathrm{d}y_2/\mathrm{d}\gamma). \tag{64}$$

These derivatives may be evaluated explicitly. For the special case of $\omega = \omega_B$ and $\gamma = 0°$ it may be seen from

Fig. 3 that $\eta = 90°$ and $d\eta/d\gamma = 0$. Equation (64) then reduces to

$$(dz_2/dy_2)_{\nu=0} = -(1 + t/d) \sin \omega_B \tan \chi/\sin 2\theta_B \quad (65)$$

where χ and ω_B are given by (16*a*) and (17*b*) respectively.

(ii) *Separation*

Equation (19) gives the solutions for γ in the diffraction plane for a crystal correctly oriented in an asymmetric position. Since the scattering vector also lies in the diffraction plane, both the incident and diffracted rays specified by these (γ,η) values lie in the diffraction plane. Substituting either solution of (19) in (8) and then both (19) and (8) in (63*a*), we get the Y_2 component of this diffracted ray at the detector for the wavelength with Bragg angle θ_B:

$$y_{2,0} = -d \tan(\theta - \theta_B) \sin(\theta_B - \varepsilon)/\sin(\theta_B + \varepsilon) - t \tan(\theta - \theta_B). \quad (66)$$

APPENDIX III
The height of the diffracted-beam envelope

The diffracted-beam envelope is given by $\gamma = \gamma_0$. The maximum and minimum in the Z_2 direction at the detector correspond to

$$d(\mathbf{P}_{d,2})_Z/d\eta = 0, \quad (67)$$

where $(\mathbf{P}_{d,2})_Z$ is given by (63*b*). Expanding (67) gives a very lengthy expression with no obvious solution for η. For small beam divergences we neglect terms of higher than first order in $\tan \gamma$ (the exact expression is cubic in $\tan \gamma$) to give

$$d(\mathbf{P}_{d,2})_Z/d\eta \simeq \cos \eta \tan \gamma_o(da^2 \cos^2 \gamma_0 + t). \quad (68)$$

The right-hand side of (68) is zero if $\eta = \pm 90°$. For $\eta = \pm 90°$,

$$(\mathbf{P}_{d,2})_Z = \pm(d + t) \tan \gamma_0 + d \tan^2 \gamma_0 \cos \chi(1 - \cos 2\theta) \times (\sin \chi \sin \omega \mp \cos \chi \tan \gamma_0)^{-1}. \quad (69)$$

If terms higher than first order in $\tan \gamma_0$ are also neglected in (69), the total height of the image at the detector is

$$h \simeq 2(d + t) \tan \gamma_0. \quad (70)$$

APPENDIX IV
An approximate expression for $W_{2\theta}$

For a correctly aligned reflection for which $\alpha_0 = 0°$ the perimeter of the cross section of the diffracted-beam envelope is very nearly a circle; for a reflection for which $\alpha_0 \neq 0°$ aligned at either of the two extreme positions of asymmetric reflection so that $\chi = 90°$, the perimeter is very nearly an ellipse with axes along Y_2 and Z_2 (see Fig. 4). In both cases the $K\alpha$ images and the images due to every wavelength are perpendicular to the diffraction plane. Consider now the general case of a reflection with $\alpha_0 \neq 0°$, aligned at any position of asymmetric reflection. The $K\alpha$ images are still nearly straight but are inclined to the diffraction plane, seemingly obtained from the images at $\chi = 90°$ by translating each point on the images parallel to the Y_2 axis by an amount proportional to the Z_2 component. Assume then that the perimeter of the cross section is obtained from an ellipse with axes $W_0/2$ and $h/2$ along Y_2 and Z_2 respectively by a similar translation of each point.

The equation of this ellipse is

$$4y^2/W_0^2 + 4z^2/h^2 = 1, \quad (71)$$

where y and z are coordinates in the Y_2Z_2 plane. The coordinates of the corresponding translated point on the cross-section perimeter are

$$y' = y + z/g \quad (72a)$$

and

$$z' = z. \quad (72b)$$

From inspection of Figs. 4 and 6 the constant g is the inclination of the lines of constant wavelength in the diffracted image, $(dz_2/dy_2)_{\nu=0}$. By solving (72) for y and z and substituting in (71) we find the equation for the perimeter:

$$4y'^2/W_0^2 + 4z'^2[1/(g^2 W_0^2) + 1/h^2] - 8y'z'/(gW_0^2) = 1. \quad (73)$$

For a particular diffractometer the accuracy of (73) as a solution to (63) should be determined over the permitted ranges of the diffractometer angles.

From evaluation of (73) for dy'/dz', the maximum and minimum in y' are

$$y' = \pm\tfrac{1}{2}[W_0^2 + h^2/g^2]^{1/2}. \quad (74)$$

Therefore, the total image width is

$$W_{2\theta} = [W_0^2 + h^2/(dz_2/dy_2)^2_{\nu=0}]^{1/2}. \quad (75)$$

References

ALEXANDER, L. E. & SMITH, G. S. (1962). *Acta Cryst.* **15**, 983–1004.

ARNDT, U. W. & WILLIS, B. T. M. (1966). *Single Crystal Diffractometry*, p. 267. Cambridge Univ. Press.

BARNEA, Z. (1975). *Anomalous Scattering*, edited by S. RAMASESHAN & S. C. ABRAHAMS, pp. 289–291. Copenhagen: Munksgaard.

BILDERBACK, D. H. & COLELLA, R. (1976). *Phys. Rev. B*, **13**, 2479–2488.

BRAGG, W. H. (1914). *Philos. Mag.* **27**, 881–899. [Reproduced in *Acta Cryst.* (1969), A**25**, 3–11.]

BURBANK, R. D. (1964). *Acta Cryst.* **17**, 434–442.
BUSING, W. R. & LEVY, H. A. (1967). *Acta Cryst.* **22**, 457–464.
DENNE, W. A. (1977*a*). *Acta Cryst.* A**33**, 438–440.
DENNE, W. A. (1977*b*). *Acta Cryst.* A**33**, 987–992.
EINSTEIN, J. R. (1974). *J. Appl. Cryst.* **7**, 331–344.
FIELD, J. E. & LINDSAY, G. A. (1937). *Phys. Rev.* **51**, 165–169.
FREEMAN, D. K., MAIR, S. L. & BARNEA, Z. (1977). *Acta Cryst.* A**33**, 355–359.
FURNAS, T. C. & HARKER, D. (1955). *Rev. Sci. Instrum.* **26**, 449–453.
GAY, P., HIRSCH, P. B. & KELLAR, J. N. (1952). *Acta Cryst.* **5**, 7–11.
HAMILTON, W. C. (1974*a*). In *International Tables for X-ray Crystallography*, Vol. IV, §3.2. Birmingham: Kynoch Press.
HAMILTON, W. C. (1974*b*). In *International Tables for X-ray Crystallography*, Vol. IV, §3.3.2. Birmingham: Kynoch Press.
HARADA, J., PEDERSEN, T. & BARNEA, Z. (1970). *Acta Cryst.* **26**, 336–344.
HOLLENBERG, W. C. & BATTERMAN, B. W. (1974). *Phys. Rev. B*, **10**, 2148–2158.
HUIJSER-GERITS, E. M. C. & RIECK, G. D. (1974). *J. Appl. Cryst.* **7**, 286–290.
KHEIKER, D. M. (1969). *Acta Cryst.* A**25**, 82–88.
LADELL, J., PARRISH, W. & TAYLOR, J. (1959). *Acta Cryst.* **12**, 561–567.
LADELL, J. & SPIELBERG, N. (1966). *Acta Cryst.* **21**, 103–118.
LIMINGA, R., CHOMNILPAN, S. & ABRAHAMS, S. C. (1978). *J. Appl. Cryst.* **11**, 128–131.
MCINTYRE, G. J. (1981). In preparation.
MCINTYRE, G. J. & BARNEA, Z. (1978). *Acta Cryst.* A**34**, S336.
MAIR, S. L. & BARNEA, Z. (1975). *J. Phys. Soc. Jpn*, **38**, 866–869.
MAIR, S. L., PRAGER, P. & BARNEA, Z. (1971*a*). *J. Appl. Cryst.* **4**, 169–171.
MAIR, S. L., PRAGER, P. & BARNEA, Z. (1971*b*). *Nature (London)*, **234**, 35.
MATHIESON, A. MCL. (1975). *Acta Cryst.* A**31**, 769–774.
MATHIESON, A. MCL. (1977). *Acta Cryst.* A**33**, 610–617.
MERISALO, M. & JÄRVINEN, M. (1978). *Philos. Mag.* B**37**, 233–240.
MERISALO, M., JÄRVINEN, M. & KURITTU, J. (1978). *Phys. Scr.* **17**, 23–25.
MERISALO, M., PELJO, E. & SOININEN, J. (1978). *Phys. Lett. A*, **67**, 80–82.
SCHULZ, L. (1949). *J. Appl. Phys.* **20**, 1030–1036.
SHARMA, B. L. (1966). *Solid State Electron.* **9**, 728–729.
TENCKHOFF, E. (1970). *J. Appl. Phys.* **41**, 3944–3948.
TRUCANO, P. & BATTERMAN, B. W. (1972). *Phys. Rev. B*, **6**, 3659–3666.
WERNER, S. A. (1972). *Acta Cryst.* A**28**, 143–151.
WHITELEY, B., MOSS, G. & BARNEA, Z. (1978). *Acta Cryst.* A**34**, 130–136.

Acta Cryst. (1981). A**37**, 119–125

High-Resolution Imaging of the Ferroelectric Perovskite $Ba_2Bi_4Ti_5O_{18}$

BY JOHN L. HUTCHISON

Department of Metallurgy and Science of Materials, University of Oxford, Parks Road, Oxford OX1 3PH, England

AND DAVID J. SMITH

High Resolution Electron Microscope, University Engineering Department, Free School Lane, Cambridge CB2 3RQ, England

(*Received* 12 *June* 1980; *accepted* 4 *September* 1980)

Abstract

The ferroelectric material $Ba_2Bi_4Ti_5O_{18}$ has been examined by high-resolution electron microscopy at 200 and 500 kV. With the directly interpretable resolution limit in each case extending to better than 2·5 Å, it was demonstrated that both the *A*-cation and *B*-cation positions could be resolved and, furthermore, that analysis of structural disorder at this level of resolution allowed an explanation of some observed lattice defects. In particular, unit shifts of a perovskite cell along a bismuthate sheet were identified as occurring in the manner previously postulated, and a Burgers vector circuit analysis around a low-angle domain boundary permitted the formulation of a model for the atomic configuration at the boundary. The implications of these observations for the study of perovskites generally are briefly discussed.

Introduction

The layered compound $Ba_2Bi_4Ti_5O_{18}$ is one of a family (Aurivillius, 1949) which are based on a regular

0567-7394/81/010119-07$01.00